



HAL
open science

The detection of old masonry tunnels as low electrical resistivity anomalies-application to one covered stream tunnel of the Cevennes Mountain region (France)

Thomas Hauquin, Quentin Mourey

► **To cite this version:**

Thomas Hauquin, Quentin Mourey. The detection of old masonry tunnels as low electrical resistivity anomalies-application to one covered stream tunnel of the Cevennes Mountain region (France). *Journal of Applied Geophysics*, 2019, 168, pp.12-23. 10.1016/j.jappgeo.2019.05.010 . hal-02436521

HAL Id: hal-02436521

<https://imt-mines-ales.hal.science/hal-02436521>

Submitted on 25 Oct 2021

HAL is a multi-disciplinary open access archive for the deposit and dissemination of scientific research documents, whether they are published or not. The documents may come from teaching and research institutions in France or abroad, or from public or private research centers.

L'archive ouverte pluridisciplinaire **HAL**, est destinée au dépôt et à la diffusion de documents scientifiques de niveau recherche, publiés ou non, émanant des établissements d'enseignement et de recherche français ou étrangers, des laboratoires publics ou privés.



Distributed under a Creative Commons Attribution - NonCommercial 4.0 International License

1 **The detection of old masonry tunnels as low electrical resistivity anomalies – Application**
2 **to one covered stream tunnel of the Cevennes Mountain region (France)**

3 Thomas Hauquin*, Quentin Mourey

4 *LGEI, IMT Mines Ales, Univ Montpellier, Ales, France*

5 **thomas.hauquin@mines-ales.fr*

6 **thomashauquin@hotmail.fr*

7

8 **Keywords:** 2D-ERT, Old masonry tunnels, Thin conductive layer, Forward modelling

9

10 **Abstract**

11 More than 70 km of old masonry tunnels covering natural streams were recently inventoried in the
12 Cevennes mountain region (France, *département du Gard*). Due to their advanced state of
13 degradation and their shallow depth, the covered stream tunnels have been responsible for several
14 surface collapses since 2012. The mapping of the trajectory of these tunnels therefore is of
15 primordial importance for the risk assessment of the affected municipalities. But only few of them
16 were mapped so far due to their difficult accessibility and their precarious stability. Consequently
17 there is a need to identify non-destructive methods for detecting them quickly from the surface of
18 the most preoccupying areas. Two ERT profiles using 48 electrodes and the Wenner-Schlumberger
19 array, under dry and wet conditions, were realized at the surface of one tunnel of which the position
20 was precisely known in order to determine the ability of the technique to detect it. Analysis of the
21 measured apparent resistivity showed an unexpected local decrease of resistivity near the tunnel
22 boundary. The inverse models performed without any filtering of the measured apparent resistivity
23 did not allow detecting any anomaly that could be interpreted as the presence of the tunnel.
24 Conversely, the inversion of a smoothed version of the apparent resistivity allows detecting a low
25 resistivity anomaly at the tunnel position. This result was quite surprising because we rather
26 expected a high resistivity anomaly due to the infinite resistivity of the tunnel atmosphere compared

27 to the surroundings. According to a study recently published by Putiška et al. (2012) on this topic and
28 to a set of forward resistivity models we conducted, this unexpected low resistivity anomaly was
29 explained to be due to the presence of a thin conductive layer around the tunnel. The fact that this
30 anomaly was unobserved after inversion of the unfiltered apparent resistivity was explained by the
31 presence of a high resistivity material (probably composed of coal) beside the thin conductive layer
32 that altered the least-squares inversion process.

33

34 **1. Introduction**

35

36 1.1. Context

37

38 The Cevennes mountain region was the locus of an intense coal mining during the 19th and 20th
39 centuries. More than 70 km of old masonry tunnels – the covered stream tunnels – were built above
40 natural streams in order to backfill the valleys with coal mine tailings and to build platforms for the
41 mining related plants. The coal mines closed but the covered stream tunnels remain foundation for
42 many houses and infrastructures.

43 Due to the progressive deterioration of the masonry, at least 3 covered stream tunnels collapsed
44 since 2012 and 2 tunnels collapsed before that at an undetermined date (two examples in Fig. 1). We
45 visited 30 of the larger covered stream tunnels and those where no collapse has yet occurred are
46 often in an advanced state of damage indicating that future collapses will probably happen.

47 According to the last estimate (Vayssade et al. 2015) more than 500 buildings would be located at
48 less than 50 m of the tunnels axes (at the surface) which are considered to be a zone of high risk.

49 However, these zones were determined with a great uncertainty. Indeed, the access to certain
50 tunnels is unsafe and requires specific equipment, so their trajectories were determined in an
51 approximate manner, in function of the tunnels entrances and exits only. Moreover, small secondary

52 tunnels whose entrances were occasionally found, but that cannot be inspected due to their size and
53 state of degradation, were ignored.

54

55 1.2. Problematic and objectives

56

57 An important issue is to identify non-destructive methods for locating precisely the tunnels positions
58 in some specific zones of interest from the surface, and in particular the smallest tunnels of which
59 the trajectory is the most uncertain.

60 Geophysical methods in general are known to be economic, rapid and effective for detecting shallow
61 cavities or openings in various geological contexts (Orfanos & Apostolopoulos, 2012). Among the
62 various geophysical techniques commonly used for detecting shallow cavities (microgravimetric,
63 magnetic, seismic or electrical methods), the 2D Electrical Resistivity Tomography (2D-ERT) was
64 selected in this study. 3D investigations were not necessary since the researched tunnels are long
65 and most of the time linear with a small slope so we can assume that this is a plane problem.

66 The ERT technique has several advantages that made it attractive in the context of the present study:
67 i) a sufficient resolution (depending on the chosen electrode array) in both the horizontal and vertical
68 direction so that cavities can be positioned vertically and horizontally, ii) it is a quite rapid technique
69 which does not require to spend a long time at the surface of the investigated areas which are prone
70 to collapse, iii) the method is sensitive to a great resistivity contrasts such as those expected to occur
71 between the tunnel atmosphere and the surrounding soil.

72 2D-ERT has already been demonstrated to be a reliable technique for the detection of metric cavities
73 in anthropic areas (Nero et al., 2016; Ioannis et al., 2002; Boubaki, 2013; Bianchi Fasani et al., 2013),
74 for the detection of mining cavities (Martinez-Pagàn et al., 2013; Bharti et al., 2016) and karsts
75 (Gómez-Ortis & Martín-Crespo, 2012; Metwaly & AlFouzan, 2013), and for the detection of shallow
76 concrete tunnels (Riddle et al., 2010). The ERT technique was also successfully used to detect
77 partially filled old shafts (Amini & Ramazi, 2016). In all cases, cavities appear as a highly resistive

78 anomaly whose inversed resistivity depends on several factors such as the cavity diameter and the
79 surrounding soil resistivity. The analysis of the published results shows that the depth of the
80 investigated cavities is accurately identified by 2D-ERT in general and that it is an appropriate
81 method of approaching the cavity extension where it is unknown.

82 Despite the significant number of publications related to the detection of shallow cavities with 2D-
83 ERT, in our best knowledge, no study was published about the detection of old masonry tunnels such
84 as the covered stream tunnels. So the present study tackled the following objectives:

- 85 • assessing the capability of 2D-ERT to detect old masonry tunnels,
- 86 • determining what type of resistivity anomaly is to be expected at the tunnel position,
- 87 • determining the conditions of a good detection.

88

89 1.3. Study plan

90

91 To answer these objectives, the study was organized as follows. First, we selected an adequate study
92 site consisting of a tunnel of which we precisely know the trajectory in order to be able to assess the
93 precision of its detection with 2D-ERT. We also identified a second tunnel in the same area that we
94 were susceptible to detect but of which we didn't know the trajectory (Section 2). Then, we realized
95 two 2D-ERT measurements along one profile perpendicular to the main tunnel axis under different
96 weather conditions. The measured apparent resistivity was inverted with the RES2DINV software
97 (Section 3). After that, we realized forward models with the RES2DMOD software with resistivity
98 values based on small scale *in situ* measurements for the purpose of giving explanation to one
99 unexpected result obtained after inversion of the measured apparent resistivity (Section 4). Finally,
100 the combined interpretation of inverse and forward resistivity models led us to draw practical
101 conclusions about the detectability conditions of old masonry tunnels with 2D-ERT (Section 5).

102

103

104 2. Method

105

106 2.1. Brief introduction of the 2D Electrical Resistivity Tomography (2D-ERT)

107

108 The 2D-ERT consists of measuring the apparent resistivity of the sub-surface by injecting a direct
109 electrical current in the ground between two electrodes A and B (current electrodes) and measuring
110 the induced voltage between two other electrodes M and N (potential electrodes). From the injected
111 current I and the measured voltage V , the average resistivity ($\Omega.m$) of the ground crossed by the
112 current, i.e. the apparent resistivity, can be calculated as:

$$113 \rho_{app} = \frac{KV}{I} \quad (1)$$

114 where K is the geometric factor calculated as:

$$115 K = \frac{2\pi}{\left[\frac{1}{MA} + \frac{1}{MB} + \frac{1}{NA} + \frac{1}{NB} \right]} \quad (2)$$

116 The positions and spacing between the electrodes are successively varied in order to measure the
117 apparent resistivity at different positions along a profile and at different depth levels.

118 From the measured apparent resistivity, an inverse model is conducted in order to estimate the true
119 resistivity values of the sub-surface responsible for the measured apparent resistivity. Variations of
120 the true resistivity are interpreted as a change of material or as a change of fluid condition within a
121 given material.

122 The relative position of the current electrodes compared to the position of the potential electrodes
123 defines the electrodes array. The most common arrays used for sub-surface investigations are the
124 Wenner array (W), the Dipole-Dipole array (DD), the Pole-Dipole array (PD), the Pole-Pole array (PP),
125 and the Wenner-Schlumberger array (WS). They differ mostly by their sensitivity to horizontal or
126 vertical structures, their noise level and their depth of investigation (see Loke, 2016 for details). The
127 apparent and inverse model resistivity both depend on the chosen electrode array.

128

129 2.2. Study site presentation

130

131 Our study site was located in Robiac-Rochessadoule (France, *département du Gard*, Fig. 2). There are
132 5 covered stream tunnels spread across the town, 2 of which having known large collapses or
133 sinkholes in recent years. In order to assess the actual state of the tunnels in an obvious risky
134 context, the municipality ordered a precise investigation of the tunnels including their precise
135 topographic survey. So we know precisely the position, trajectory and depth of the tunnels.

136 Among the 5 covered stream tunnels, we selected the one with the most favorable features
137 regarding the study objectives: the *Rochessadoule* tunnel (Fig 3). The tunnel is about 370 m long and
138 consists of a semi-circular vault of 2.5 m radius relying on vertical sidewalls of about 1 m width and
139 1.5-2 m height. It is located under an easily accessible planar ground, with a quite homogeneous soil
140 at the surface. The accessible ground length perpendicular to the tunnel axis is about 50 m, which
141 allows having a sufficient distance between the electrodes for the depth of investigation (from 7 to
142 10 m depending on the chosen electrodes array) to be compatible with the tunnel depth (from 3 to 6
143 m depending on the distance from the tunnel entrance). Furthermore, the entrance of a small
144 secondary tunnel of 1.2 m height was found next to the main tunnel entrance. We did not know its
145 trajectory because it is partially collapsed and inaccessible a few meters after the entrance. But its
146 entrance is almost parallel to that of the main tunnel, so we expected that would be able to detect it
147 somewhere along the resistivity profiles.

148 We did not know the precise composition of the investigated soil. However, at least five material
149 types were supposed to be present in the investigated zone:

- 150 • a thin homogenous layer of silt at the ground surface with an heterogeneous water
151 saturation,
- 152 • a heterogeneous backfill material composed of coal mine tailings around the tunnel,
- 153 • an old masonry of 0.5 to 1 m width forming the tunnel structure, mostly composed of
154 Triassic sandstone and mortar or concrete joints,

- 155 • the host rock of the tunnel composed of Triassic sandstone, and
- 156 • the atmosphere of the tunnel.

157

158 The atmosphere of the tunnel is supposed to have a very high, say infinite, resistivity compared to
 159 the other material types. The resistivity of the other material types was estimated *in situ* thanks to
 160 small scale electrodes arrays. The backfill material surrounding the tunnel was not directly accessible
 161 so its resistivity was estimated in a pile of unused material stored next to the studied sector (Fig. 4a).
 162 We supposed that the same material was used during the tunnel construction. The resistivity of the
 163 masonry was determined thanks to a 1D horizontal sounding realized by inserting small screws at the
 164 surface of the tunnel sidewall. Similarly, a horizontal sounding was realized on the vertical surface of
 165 the host rock flushing near the tunnel entrance. Table 1 summarizes the resistivity values obtained
 166 by averaging the result of various depths of investigation inside the *in situ* materials (from 25 cm to 1
 167 m in the rock, the masonry and the backfill; from 10 cm to 50 cm in the silt layer).

168

169 **Table 1:** estimated *in situ* resistivity of the materials we were supposed to detect with the ERT.

Material	Tunnel Atmosphere	Silt	Backfill	Host rock	Masonry
Estimation of <i>In situ</i> resistivity ($\Omega.m$)	∞	≈ 100	≈ 250	≈ 700	≈ 500

170

171 2.3. ERT profiles characteristics

172

173 The ERT profile (Fig. 4b) was placed so that the main tunnel axis was in the center of the profile (Fig.
 174 2b) and the tunnel depth was of about 3.3 m. In this way, the contour of the tunnel theoretically was
 175 comprised within the measurement profile. We used a unit (minimal) electrode spacing of 1 m and

176 48 electrodes, so the measurement profile was of 47 m length. We selected the WS array, which is an
177 interesting compromise between the W and the DD arrays (Loke, 2016) offering a sufficient depth of
178 investigation (about 9 m), a moderate noise level (Dahlin et al., 2004) and a sensitivity similar in
179 horizontal and vertical directions. This latter point was of primordial importance since we were
180 dealing with a ground with both a vertical stratification and a horizontal variation of resistivity due to
181 the presence of the tunnel.

182 The WS technique consists of a symmetrical electrodes array. The potential electrodes (M and N) are
183 placed in the middle with a spacing a and the current electrodes (A and B) at a distance of $n \times a$ from
184 the potential electrodes, where n is a positive integer. The unit spacing a is first kept constant while n
185 is successively increased. Then, a is increased and kept constant again while n is successively
186 increased. This procedure is reproduced until the maximum depth of investigation; depending on the
187 maximum array length, is reached.

188 A WS sequence comprising 621 acquisition points (quadripoles) was programmed. It was composed
189 of 9 values of a , from 1 m to 9 m, and 3 depth levels n for every value of a . Fig. 5 represents the
190 position of the median depth of investigation of all the 621 acquisition points.

191 The acquisition points almost overlap vertically every three lines, which are thus characterized by a
192 better resolution than the other lines. Comparison of the apparent resistivity of overlapping points is
193 a good way of checking the robustness of the resistivity measure and the eventual effect of noise.

194 Two acquisitions were realized along the same profile: the first one (25 May 2017) under dry
195 conditions (less than 1 mm of precipitation cumulated during the past week) and the second one (30
196 June 2017) under wet conditions (about 30 to 40 mm of precipitation cumulated during the past 3
197 days), both using the *Syscal Junior Switch 48* resistivity meter. The following injection parameters
198 were used: impulsions of 500 ms, a constant reception voltage of 50 mV and a maximum injected
199 voltage of 400 V. The number of stacks was between 4 and 10 with an objective coefficient of
200 variation of 1%.

201

202 3. Resistivity models

203

204 3.1. Apparent resistivity measurements

205

206 First of all, note that the measured apparent resistivity shows small coefficients of variation
207 regardless of the depth of level and the position along the profile. Fig. 6 shows the coefficient of
208 variation of every data point. The average coefficient of variation is of $\approx 0.22\%$ under both wet and
209 dry conditions, while the maximum coefficient of variation is of $\approx 5\%$ and is obtained only in the first
210 depth level. Moreover, only 4 stacks were necessary most of the time, what means that the
211 measurement were relatively little noisy. Otherwise, no aberrant data points were found, so the
212 measured apparent resistivity did not need to be filtered *a priori*.

213 In order to illustrate the major trends of the apparent resistivity, let us analyze the measurements
214 along two perpendicular profiles: a vertical profile at mid tunnel span and a horizontal profile
215 crossing at mid tunnel height. On both profiles, we calculated the average apparent resistivity
216 corresponding to all the data points at a given level perpendicular to the profiles. Fig. 7a shows the
217 results of the vertical profile corresponding to the evolution of the apparent resistivity in function of
218 the median depth of investigation. Fig. 7b shows the results along the horizontal profile
219 corresponding to the evolution of the apparent resistivity in function of the position of the potential
220 electrodes center along the measurement profile.

221 The following points must be noticed concerning the vertical profile (Fig. 7a):

- 222 • Overall, the apparent resistivity increases with the depth, what is more visible under wet
223 conditions than under dry conditions.
- 224 • Regardless of the water conditions, the smallest apparent resistivity is observed near the
225 surface (silt layer) while the greatest resistivity is observed inside the tunnel, which is
226 compatible with the resistivity estimated in Table 1.

- 227 • The top of the vault (masonry) matches the depth at which the difference between the wet
228 and dry apparent resistivity is the smallest.
- 229 • The apparent resistivity slightly decreases near the top of the masonry (vault) after
230 increasing again inside the tunnel atmosphere. This decrease is incompatible with the
231 material resistivity estimated in Table 1. Indeed, the masonry is supposed to be more
232 resistive than the backfill material above the tunnel.

233 The following points must be noticed concerning the horizontal profile (Fig. 7b):

- 234 • Overall, the apparent resistivity increases with the proximity to the tunnel, which is
235 compatible with the resistivity of Table 1.
- 236 • However, there is a local decrease and then a local pic of the apparent resistivity near the
237 tunnel boundaries that cannot be explained according to the resistivity of Table 1.

238

239 An explanation of the unexpected resistivity decrease near the masonry in both the vertical and
240 horizontal directions will be proposed in Section 4.

241

242 3.2. Inverse resistivity model

243

244 3.2.1 Inversion method selection

245

246 Many distributions of the true ground resistivity can induce the same measured apparent resistivity;
247 there is non-uniqueness of the solution. Inversion consists in determining one unique ground
248 resistivity distribution in function of the apparent resistivity distribution. To do that, a model of
249 ground resistivity distribution is postulated (homogeneous in general) and the apparent resistivity
250 that would be obtained with such a distribution is calculated using finite element or finite difference
251 method. The difference between the measured and calculated apparent resistivity is determined
252 (RMS error). Then the model resistivity distribution is iteratively changed until the relative difference

253 between the calculated and measured apparent resistivity is lower than an objective RMS error value
254 fixed arbitrary (in general from 1% to 5%).

255 The way the resistivity of the model is iteratively modified to fit the measured apparent resistivity
256 depends on the chosen norm of inversion. There are 2 common norms (Loke, 2016): the smoothness
257 constrained least-squares method (l2-norm) and the robust method (l1-norm, Claerbout & Muir,
258 1973), also based on the least-squares method. The robust inversion is supposed to be used where
259 there is great resistivity contrasts over short distances. Such contrast was supposed to occur
260 between the masonry ($\approx 500 \Omega.m$) and the tunnel atmosphere (∞), so the robust method proposed
261 by the RES2DINV software was selected.

262 Such as it is commonly recommended (Loke, 2016) the logarithm of the resistivity values was used
263 instead of the resistivity itself for the results to be in a linear scale (instead of its natural logarithmic
264 scale) which is more easily represented on the profiles.

265 To solve the (calculated) apparent resistivity in function of the resistivity model during inversion, we
266 used the finite element method with a square mesh of constant size equal to the unit electrode
267 spacing (1 m). Resistivity models were then composed of 481 blocks (Fig. 8).

268

269 3.2.2 Inversion of the unfiltered apparent resistivity

270

271 During inversion, the RMR error turned out to rapidly decrease over the iteration process. Seven
272 iterations were sufficient to obtain an error of less than 1.5% in both wet and dry conditions, which
273 matches the range typically recommended of 1% to 5% (Loke, 2015). The inversion results are
274 presented in Fig. 8 with the position of the tunnel determined beforehand according to plans with an
275 imprecision of less 0.5 m.

276 Note first that the inverse resistivity models under wet and dry conditions are qualitatively similar.

277 There is no structure that we can detect only under a specific condition.

278 The ranges of resistivity expected for the investigated materials were effectively obtained. The
279 inverted resistivity close to the surface in the silt layer ranges from 20 Ω .m in zones where the soil
280 was observed to be saturated of water to 200 Ω .m in dry zones, which is around the expected
281 average resistivity of about 100 Ω .m (Table 1). The inverted resistivity of the backfill material under
282 the silt layer is quite heterogeneous but ranges from 200 to 350 Ω .m for an expected resistivity of
283 250 Ω .m (Table 1). But surprisingly, the tunnel boundaries were not detected on the inverse models
284 under both wet and dry conditions. Indeed, even if there was a higher resistivity of about 400 Ω .m
285 near the tunnel position that could match the resistivity expected for the tunnel masonry (500 Ω .m,
286 Table 1), the tunnel contours could not be clearly identified. Moreover, the expected highly resistive
287 anomaly in the position of the tunnel center was not obtained. Such a highly resistive anomaly
288 appeared horizontally aligned with the tunnel center, but it was not correctly positioned vertically
289 and its size was lower than the tunnel size (dark red anomaly, Fig. 9).

290

291 3.2.3 Inversion of the filtered apparent resistivity

292

293 The measured apparent resistivity was not initially filtered because no aberrant data were visible and
294 the data point's coefficients of variation were small. However, the data show large differences
295 between two successive points. We supposed that this scattering, which was not considered as an
296 artifact *a priori*, was at the origin of the non-detection of the tunnel with the inverse models.
297 Therefore, we applied to the measured apparent resistivity the automatic average median filter
298 followed by the automatic sliding mean filter proposed by the PROSYSII software (Iris Instrument,
299 France). These filters consist in smoothing the measured apparent resistivity horizontally, i.e. along
300 the lines corresponding to every depth levels successively, by changing the resistivity of every data
301 point to be equal to the median and the arithmetic mean of the neighbor data points respectively.
302 The neighbor data points used for the smoothing were selected within a distance of 1 x AM around
303 the considered data point for the sliding median and 0.5 x AM around the considered data point for

304 the sliding average (PROSYSII software recommendation), where AM is the distance between the
305 closest injection (A) and potential electrodes (M).

306 The resulting apparent resistivity is vertically similar but horizontally smoother than the unfiltered
307 one (Fig. 10b). It keeps the overall same trends except that the pics of resistivity observed at
308 positions of 13 m and 37 m were significantly smoothed (Fig. 10b).

309 On the image obtained after inversion (Fig. 11), it is surprising to see that the main tunnel now
310 clearly appears as one anomaly of low resistivity ($\approx 70 \Omega.m$) in comparison with the surrounding
311 material (300 to 400 $\Omega.m$) while there is still a high apparent resistivity at the tunnel position (Fig.
312 10b). The tunnel boundaries now are detected with a relatively good precision both in the vertical
313 and horizontal directions. Indeed, the top of the anomaly coincides with the top of the vault, the
314 center of the low resistivity anomaly nearly is in the center of the tunnel and the size of the anomaly
315 is of the same order as the tunnel width.

316 Note that the water condition has no significant effect on the main tunnel detection. However, under
317 wet conditions (Fig. 11a), a low resistivity anomaly of smaller size appears at $x \approx 36$ m. This anomaly
318 is adequately positioned (correct side compared to the main tunnel and correct altitude) to be
319 interpreted as the effect of the small secondary tunnel whose precise position is actually unknown.
320 However, the fact that this anomaly does not appear under dry conditions (Fig. 11b) could invalidate
321 this interpretation.

322 Sections 4.1 and 4.2 will respectively discuss the origin of the low resistivity anomaly at the main
323 tunnel position and the effect of the smoothing filter on the detection of this anomaly. The possible
324 detection of the small secondary tunnel under wet conditions will be discussed in section 4.3.

325

326 **4. Discussion of the results**

327

328 4.1 Detection of the main tunnel

329

330 4.1.1 Preliminary assumptions

331

332 As expected, the covered stream tunnel can be successfully detected using the 2D-ERT technique.

333 But surprisingly, the tunnel is detected as a low resistivity anomaly instead of a high resistivity

334 anomaly on the inversed models. A high resistivity anomaly would have been easily explained by the

335 very high resistivity of the tunnel's atmosphere compared to the surrounding materials, which is not

336 in doubt. Conversely, explaining the low resistivity anomaly is not immediate especially since a high

337 resistivity anomaly does appear on the apparent resistivity profile but disappears after inversion.

338 According to Putiska et al. (2012) such low resistivity anomaly can be explained by the presence of a

339 thin layer of relatively conductive material around the tunnel that would deform the resistivity image

340 after inversion. This layer can be composed of water, moisture and clay particles deposited by

341 seepage water. The effect of such a layer was demonstrated by the authors according to synthetic

342 forward resistivity models considering circular cavities without masonry. They showed that the ratio

343 of the thin conductive layer resistivity to the surrounding soil resistivity has to be of at least 0.1 for

344 the cavity to be properly detected.

345 In order to verify the validity of Putiska's results in the case of the old masonry tunnels we were

346 studying, forward resistivity models were conducted with the RES2DMOD software (Loke, 2014).

347 Forward resistivity modelling aims to evaluate the apparent resistivity that would be measured and

348 the inverse resistivity model that would be obtained with it considering a given "true" ground

349 resistivity distribution (resistivity model) and a given electrode array.

350

351 4.1.2 Forward modelling considering a uniform surrounding

352

353 We constructed a resistivity model with tunnel geometry as close as possible from the true tunnel

354 geometry. However, we considered an intentionally simplistic geometry of the surrounding materials

355 (Fig. 12). The objective was first to evaluate the detectability of the tunnel as a low resistivity
356 anomaly where it is surrounded by a homogenous and uniform material.

357 To do so, the resistivity of the backfill, the rock and the masonry was fixed according to Table 1 and
358 the resistivity of the atmosphere was fixed at 100 000 $\Omega\cdot\text{m}$ (infinite relatively to the other materials).
359 The resistivity of the thin conductive layer around the masonry was logarithmically varied from 0.01
360 to 10 $\Omega\cdot\text{m}$. The voltage that would be measured with a WS array at the surface and a unit electrode
361 spacing of 1 m was calculated, as well as the apparent resistivity, with the RES2DMOD software. Then
362 the measured apparent resistivity was inverted with the RES2DINV software considering the settings
363 described in section 3.2.1.

364 The obtained inverse resistivity model was compared to that obtained considering the field
365 measurement (section 3.2.3) along two profiles: a vertical line crossing the tunnel at mid-span and a
366 horizontal line crossing the tunnel at mid-height. The results are synthetized in Fig. 13.

367 With no conductive layer, the tunnel appears as a highly resistive anomaly. With a thin conductive
368 layer of 10 $\Omega\cdot\text{m}$ resistivity, the tunnel is detected as an anomaly of slightly higher resistivity than the
369 surroundings (red curves) in both the horizontal (Fig. 13a) and vertical directions (Fig. 13b). With a
370 thin layer resistivity lower than 1 $\Omega\cdot\text{m}$, the tunnel is detected as an anomaly of lower resistivity than
371 the surroundings. The ratio of the thin layer resistivity to the surroundings resistivity for the tunnel to
372 be detected as a low resistivity anomaly therefore is of about 0.004. But for the low resistivity
373 anomaly to be of the same order as that obtained considering the field measurements ($\approx 70 \Omega\cdot\text{m}$), the
374 thin layer resistivity has to be in the range of 0.01 to 0.1 $\Omega\cdot\text{m}$. The corresponding resistivity ratio is of
375 about 0.0002. This ratio cannot be directly compared to that proposed by Putiška et al. (2012) since
376 the model geometry was different. Nevertheless, the description of the effect of a thin conductive
377 layer around the tunnel such as proposed by Putiška et al. (2012) is qualitatively verified here.

378

379 4.1.3 Forward modelling considering a more realistic surrounding

380

381 Despite the good agreement between the resistivity obtained at the tunnel position after inversion of
382 the measured and modelled apparent resistivity, the resistivity obtained outside the tunnel did not
383 fit well the expected resistivity horizontally (Fig. 13a) or vertically (Fig. 13b). This was probably due to
384 the simplistic flat geometry we considered for the rock under the tunnel. Actually, the tunnel was
385 built inside an incised valley, so the rock is supposed to form slopes on both sides of the tunnel. The
386 exact slope is unknown since the rock is fully covered by backfill materials, and it is probably not a
387 regular slope. However, in order to simply take it into account in the forward models, we considered
388 a regular slope of alternatively 20°, 45° and 70° (the model with a slope angle of 70° is presented in
389 Fig. 14). The resistivity of the thin conductive layer was fixed at 0.01 Ω .m.

390 Once again, the obtained inverse resistivity model was compared to that obtained considering the
391 field measurement (section 3.2.3) along two profiles: a vertical line crossing the tunnel at mid-span
392 and a horizontal line crossing the tunnel at mid-height. The results are synthetized in Fig. 15.

393 Along the horizontal profile (Fig. 15a) increasing the rock slope has several consequences. First, the
394 resistivity from the forward models inside and outside of the tunnel fits better the resistivity from
395 the measured apparent resistivity. Secondly, the resistivity decrease near the tunnel boundary is
396 steeper and closer to that obtained with the measured apparent resistivity. Thirdly, however, the
397 limits of the anomaly are in a less good agreement with the inverted resistivity obtained considering
398 the field measurements: the size of the tunnel is overestimated.

399 Along the vertical profile (Fig. 15b) increasing the rock slope has less consequence. Due to adding a
400 layer of low resistivity material representing a silt layer at the surface, the resistivity curve near the
401 top of the vault has a shape that is more similar to the expected shape. However, the intensity of the
402 resistivity does not fit the expected intensity better.

403 Overall, the presence of a rock slope besides the tunnel boundaries increases the intensity of the
404 lowly resistive anomaly compared to the surroundings after inversion of the apparent resistivity.

405 Still, the forward models we conducted did not explain why we needed to smooth the measured
406 apparent resistivity by applying sliding filters to be able to detect the tunnel on the image obtained
407 after inversion. Justifications of that point are provided in the next section.

408

409 4.2 The effect of the smoothing filter

410

411 The main tunnel only was detected after the apparent resistivity was smoothed according to a sliding
412 average and a sliding median filter. One could have thought that the measured apparent resistivity
413 was submitted to noise, which was attenuated thanks to the smoothing filter. But the fact that this
414 observation was similarly made on both sides of the tunnel and considering two separate
415 acquisitions, under wet and dry conditions, realized one month apart, shows that this is probably not
416 due to a random noise.

417 The main difference between the filtered and the unfiltered apparent resistivity that appears on the
418 horizontal profile (comparison of Figs. 7b and 10b) is the smoothing of the pic of resistivity besides
419 the tunnel lateral boundaries (at 13 m and 37 m along the horizontal profile). So the following
420 explanation can be proposed.

421 Without applying the smoothing filter, no clear highly resistivity anomaly was visible at the tunnel
422 position because of the presence of pics of resistivity a few meters beside the tunnel boundaries.
423 Consequently the tunnel contours cannot be precisely viewed on the inversion image.

424 There was no clear low resistivity anomaly neither because the effect of the thin conductive layer,
425 which is visible on the apparent resistivity profile (at positions of 14 m and 35 m in Fig. 7b),
426 disappears after inversion. It is probably due to the fact that the effect of the conductive layer
427 significantly affects the apparent resistivity over a too short horizontal distance to induce a resistivity
428 decrease during the least square inversion process.

429 Conversely, after applying the smoothing filter, the pics of resistivity a few meters beside the tunnel
430 boundaries disappear and the presence of the thin conductive layer now is fictively characterized by

431 an approximately constant apparent resistivity beside the tunnel boundaries (contoured zones in Fig.
432 7b). The effect of the thin conductive layer is significant, in this case, over a sufficient distance so that
433 it forces the least square process to decrease the resistivity at the tunnel position for the calculated
434 apparent resistivity to fit the measured apparent resistivity.

435 We have no direct measurement of what can induce the pics of apparent resistivity. However, we
436 can reasonably make the following supposition.

437 It was occasionally observed on various covered stream tunnels that a layer of thin backfill material
438 mostly composed a coal particles was deposited around the masonry before the deposit of a
439 progressively coarser backfill material up to the final altitude. Such a construction method was
440 probably used to assure a uniform loading of the vault. The presence of a layer of backfill material
441 mostly composed of coal near the masonry with a relatively high resistivity of about 3000 Ω .m (we
442 estimated it thanks to a small scale *in situ* measurement) compared to the surroundings could be
443 responsible for the pic of resistivity observed in the horizontal profile of apparent resistivity (Fig. 7b).

444

445 4.3 Detection of the small secondary tunnel

446

447 A small anomaly of low resistivity, which can be interpreted as the presence of the small secondary
448 tunnel, appears on the inversion image under wet conditions only (Fig. 11a). Because the main tunnel
449 was demonstrated to be detectable under both wet and dry condition, we suppose that the small
450 anomaly of low resistivity is, this time, probably not due to the presence of a thin conductive layer
451 around the small tunnel. But the presence of the highly resistive tunnel atmosphere should at least
452 induce a highly resistive anomaly at the small tunnel position, which is not observed either. So, we
453 came to the following conclusions.

454 The small secondary tunnel is probably partially collapsed. Under dry conditions, the resistivity
455 contrast between the tunnel and the surrounding soil therefore is probably too low to be detected.

456 But under wet conditions, the small secondary tunnel probably is a preferential flow path due to its

457 very shallow depth (less than 2 m). So its resistivity probably decreases due to the presence of water,
458 making it detectable with 2D-ERT.

459

460 **5. Conclusions**

461

462 In general, the presence of subsurface cavities is expected to be detected as a highly resistive
463 anomaly on 2D-ERT profiles because of the very high (say infinite) resistivity of the cavity
464 atmosphere. But according to the results we obtained while conducting 2D-ERT profiles above an old
465 masonry tunnel of known position, cavities can also be detected as low resistivity anomalies or
466 eventually undetected under certain conditions. Anomalies of low resistivity on the inverse resistivity
467 section can be due to the presence of a thin conductive layer around the tunnel induced by the
468 presence of moisture and seepage water deposits. This effect was demonstrated based on forward
469 resistivity models performed by Putiška et al. (2012). In this study, we confirmed this effect based on
470 *in situ* resistivity measurements.

471 According to the obtained results, three situations can be encountered:

- 472 • If the tunnel has no conductive layer around the masonry, it will appear as a highly resistive
473 anomaly after inversion of the apparent resistivity.
- 474 • If the tunnel masonry is in contact with a thin layer of very low transversal resistivity
475 compared to the surroundings, it will appear as low resistivity anomaly after inversion of the
476 apparent resistivity provided that an adequate electrode array and inversion method are
477 selected.
- 478 • If the tunnel is surrounded by a highly resistive material, it will not be unconditionally
479 detected even in the presence of a conductive layer in contact with the masonry.

480 In this study, we encountered the third situation: a highly resistive anomaly was observable at the
481 tunnel position on the apparent resistivity profiles but it could not be properly detected on the
482 inversed resistivity image. The problem was solved by filtering the measured apparent resistivity with

483 a sliding median and a sliding average whose smoothing distance increases with the depth level. But
484 after filtering, the inverse resistivity image showed a low resistivity anomaly at the precise tunnel
485 position instead of an expected highly resistive anomaly. The detection of the considered tunnel was
486 successful, but there is no evidence that this method can be generalized. In addition, this is probably
487 not a satisfying option to modify the apparent resistivity by applying a filter while it did not need to
488 be filtered *a priori*.

489 Otherwise, the detection of a small secondary tunnel, of which we did not know the precise location
490 *a priori*, turned out to be possible only under wet conditions (after several days on moderate rain),
491 which is probably due a partial collapse of the tunnel.

492 Overall, the detection of old masonry tunnels with the 2D-ERT technique associated to the classical
493 least-squares method of inversion (l1-norm here) turns out to be a complex problem that can be due
494 to both the measured apparent resistivity and/or the inversion process. Further studies should
495 therefore be conducted in order to better constrain the detectability conditions of old masonry
496 tunnels using 2D-ERT, which is nevertheless a technique with many advantages.

497

498 **Acknowledgements**

499

500 We would like to thank BpiFrance, the European Union (FEDER-FSE program) and *la region Occitanie*
501 for the financial support of the research project FUI 22 EREDOS n°LR0012285. We are also grateful to
502 Dr. David Salze for the project coordination, to Mr. Thibault Jeannin for material assistance and to
503 Mr. Henri Chalvidan and the municipality of Robiac-Rochessadoules for their collaboration.

504

505

506

507

508

509 **References**

510

511 Amini, A., Ramazi, H., 2016. Application of Electrical Resistivity Imaging for Engineering Site
512 Investigation. A case Study on Prespective Hospital Site, Varamin, Iran. *Acta Geophysica*. 64(4), 2200–
513 2213.

514 Bharti, A.K., Pal, S.K., Priyam, P., Pathak, V.K., Kumar, R., Ranjan, S.K., 2016. Detection of illegal mine
515 voids using electrical resistivity tomography: The case-study of Raniganj coalfield (India). *Eng. Geol.*
516 213, 120–132.

517 Bianchi Fasani, G., Bozzano, F., Cardarelli, E., Cercato, M., 2013. Underground cavity investigation
518 within the city of Rome (Italy) : A multi-disciplinary approach combining geological and geophysical
519 data. *Eng. Geol.* 152, 109–151.

520

521 Boubaki, N., 2013. Détection de cavités par deux methodes géophysiques : radar de sol et mesures
522 de résistivités électriques. *Earth Sciences PhD. Thesis. Université Paris Sud–Paris XI; Université*
523 *d’Alep.*

524 Claerbout, J.F., Muir, F., 1973. Robust modeling with erratic data. *Geophysics*. 38(5), 826–844.

525

526 Dahlin, T., Zhou, B., 2004. A numerical comparison of 2D resistivity imaging with 10 electrode arrays.
527 *Geophysical Prospecting*. 52, 379–398.

528 Gómez-Ortiz, D., Martín-Crespo, T., 2012. Assessing the risk of subsidence of a sinkhole collapse using
529 ground penetrating radar and electrical resistivity tomography. *Eng. Geol.* 149–150, 1–12.

530 Ioannis, F.L., Vassilios, K.K., Antonio, P.V., Filippos, I.L., 2002. Resistivity modelling and imaging
531 methods for mapping near-surface features: Application to a site characterization at the ancient
532 Temple of Olypian Zeus in Anthens. *Journal of the Balkan Geophysical Society*. 5(4), 135–144.

533 Levesque, E. for Objectif Gard, October 2014. <http://www.objectifgard.com/2014/10/27/fait-du-jour->
534 [le-bassin-minier-dales-menace-deffondrement/](http://www.objectifgard.com/2014/10/27/fait-du-jour-le-bassin-minier-dales-menace-deffondrement/). Consulted in October 2018.

535 Loke, M.H., 2014. RES2DMOD ver. 3.01. Rapid 2D resistivity forward modeling using the finite-
536 difference and finite-element methods. Geotomo Software.

537 Loke, M.H., 2015. RES2DINVx64 ver. 4.05. Rapid 2-D Resistivity & IP inversion using the least-squares
538 method. Geotomo Software.

539 Loke, M.H., 2016. Tutorial 2-D and 3-D electrical imaging surveys.

540 Martínez-Pagán, P., Gómez-Ortis, D., Martín-Crespo, T. Manteca, J.I., Rosique, M., 2013. The
541 electrical resistivity tomography method in the detection of shallow mining cavities. A case study on
542 the Victoria Cave, Cartagena (SE Spain). *Eng. Geol.* 156, 1–10.

543 Metwaly, M., AlFouzan, F., 2013. Application of 2-D geoelectrical resistivity tomography for
544 subsurface cavity detection in the eastern part of Saudi Arabia. *Geoscience Frontiers.* 4, 469–476.

545 Nero, C., Aning, A.A., Danuor, S.K., Noye, R.M., 2016. Delineation of graves using electrical resistivity
546 tomography. *Journal of Applied Geophysics.* 126, 138–147.

547 Orfanos, C., Apostolopoulos, G., 2012. Analysis of different geophysical methods in the detection of
548 an underground opening at a controlled test site. *Journal of the Balkan Geophysical Society.* 15(1), 7–
549 18.

550 Putiška, R., Nikolaj, M., Dostál, I., Kušnirak, D., 2012. Determination of cavities using electrical
551 resistivity tomography. *Contributions to Geophysics and Geodesy.* 42(2), 201–211.

552 Riddle, G.I., Hickey, C.J., Schmitt, D.R., 2010. Subsurface Tunnel Detection Using Electrical Resistivity
553 Tomography and Seismic Refraction Tomography: A Case Study. *Symposium on the Application of*
554 *Geophysics to Engineering and Environmental Problems:* pp. 552–562.

555 Vayssade, B., Ayrat., P.A., Salze, D., Benzazat, I., 2016. Développement d'une méthode de
556 hiérarchisation des travaux de confortement des ruisseaux couverts prenant en compte les enjeux du
557 territoire et les risques associés. Rapport final, ARMINES, Ecole des Mines d'Alès.

558



559

560

561

562

563

Fig. 1: a) Photograph of a ≈ 25 m diameter sudden collapse occurred in 2012 in Robiac-Rochessadoules (Gard, France, picture by Levesque, 2014). b) Photograph of a large collapsed sinkhole (≈ 20 m height) occurred at an indeterminate date in La Grand-Combe (Gard, France, photographed during summer 2017).



564

565

566

Fig. 2: Study site and ERT profile location.



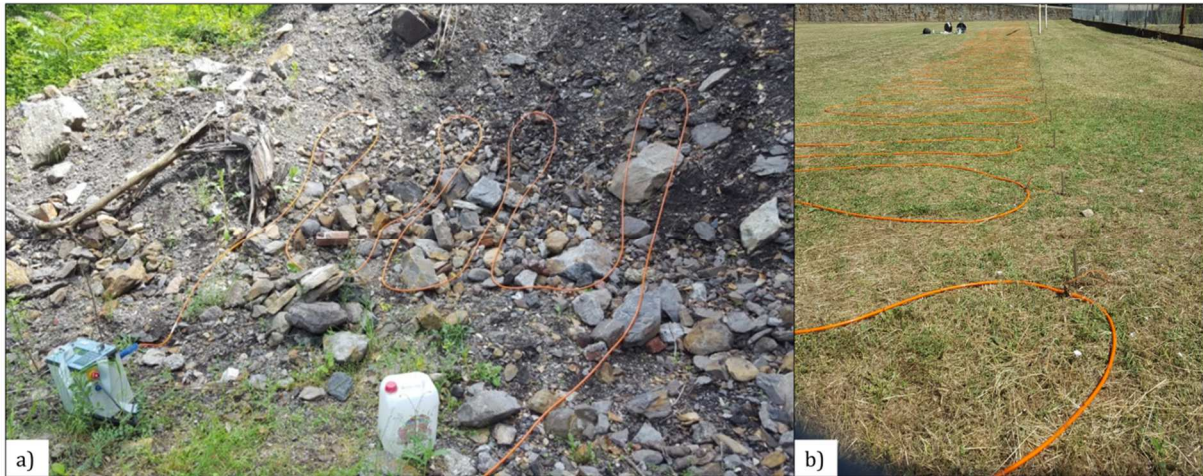
567

568

569

Fig. 3: Photographs of the entrance of the Rochessadoules covered stream tunnel (Robiac-Rochessadoules, Gard, France, taken during summer 2017): a) from the outside and b) from the inside.

570



571

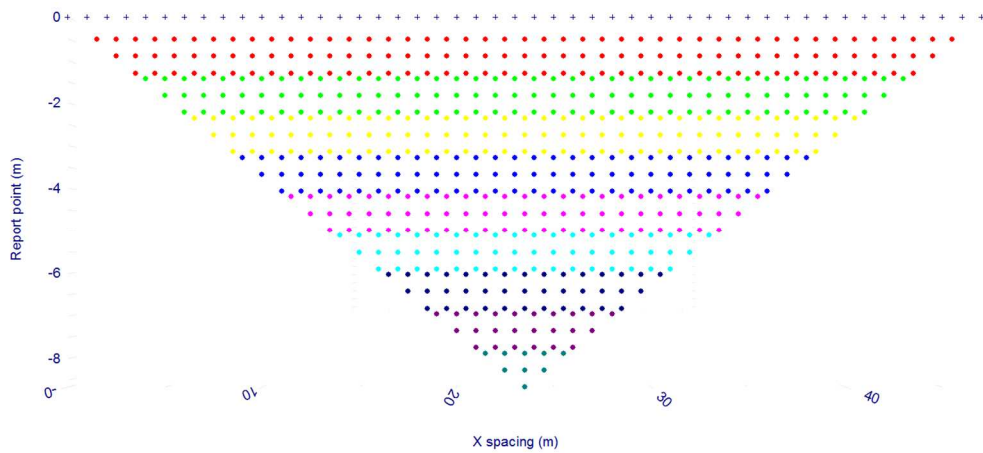
572

573

574

575

Fig. 4: a) 4-electrodes array used for the measurement of the *in situ* resistivity of a pile of coal mine tailings located near the studied tunnel, b) 48-electrodes array used for the measurement of the apparent resistivity of the ground above the studied covered stream tunnel.



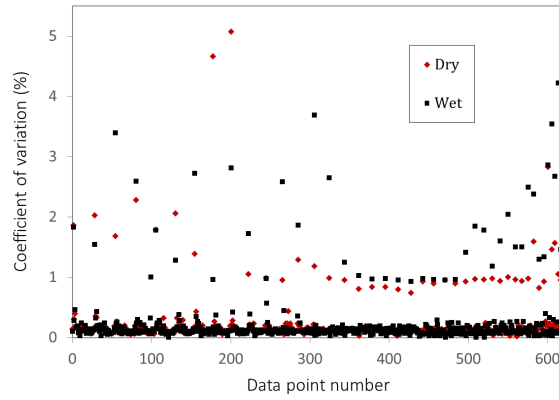
576

577

578

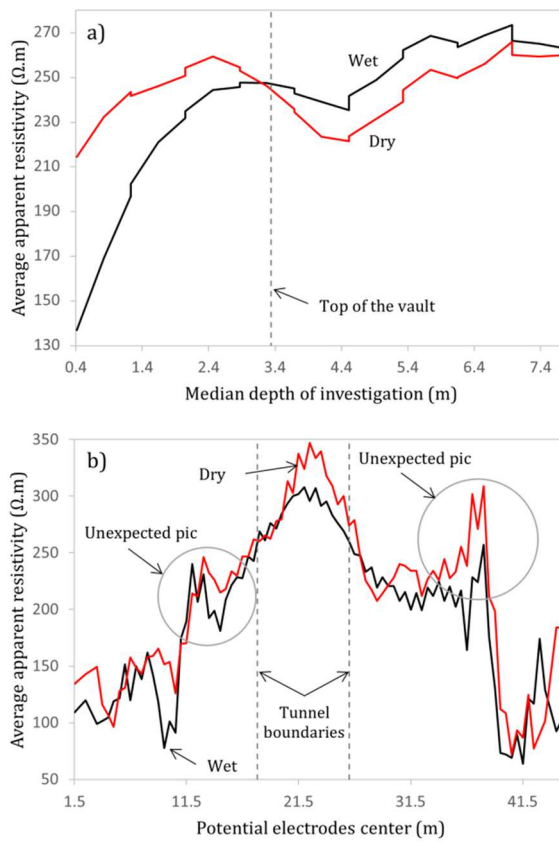
579

Fig. 5: Data points position of the ERT profiles. The position along the x axis represents the center of the quadripoles while the position along the y axis represents the median depth of investigation.



580

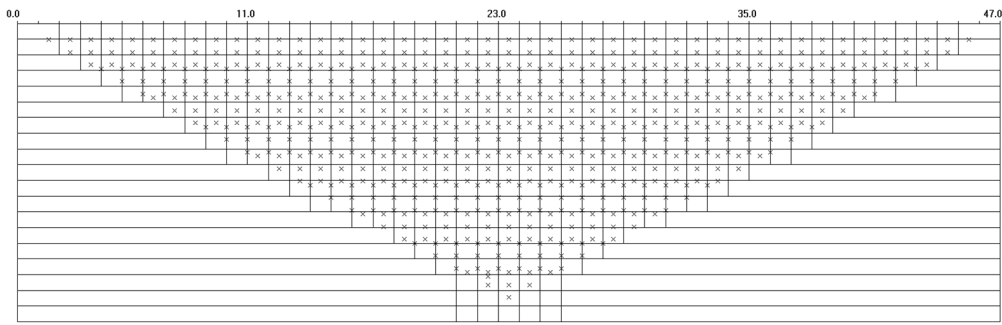
581 **Fig. 6:** Coefficient of variation of the measured apparent resistivity considering the successive stacks performed
 582 for every data point (quadripole).



583

584 **Fig. 7:** Evolution of the averaged measured apparent resistivity in function of a) the median depth of
 585 investigation and b) the potential electrodes center.

586

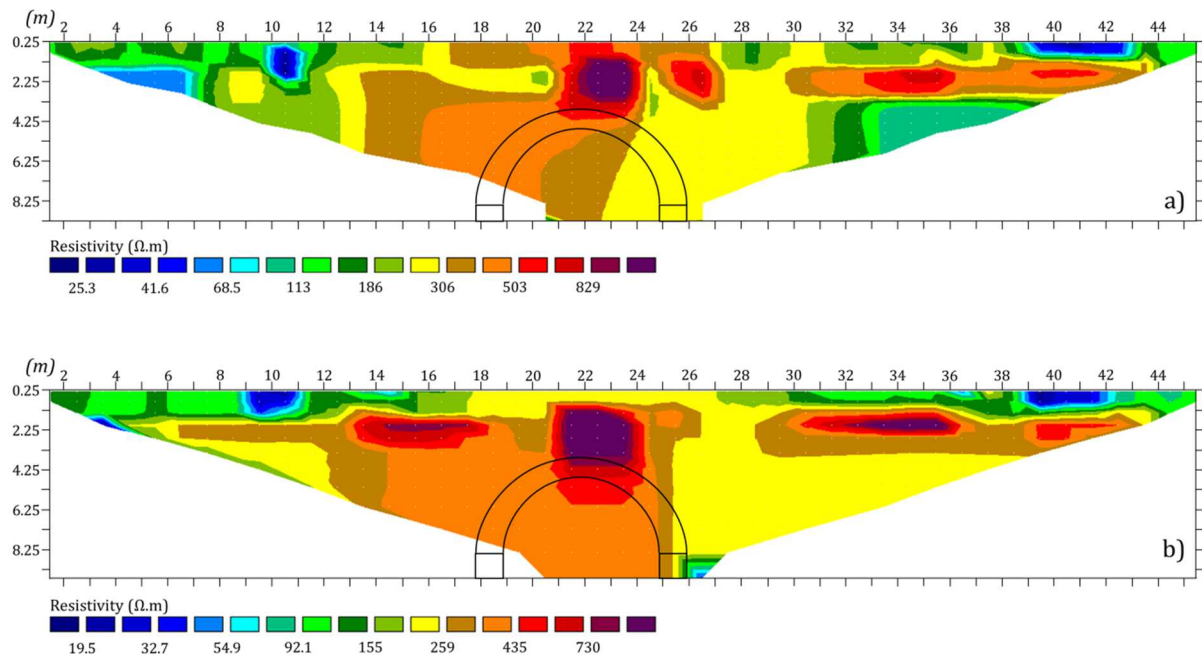


587

588

Fig. 8: RES2DINV grid of the finite element model considered for the inversion process.

589



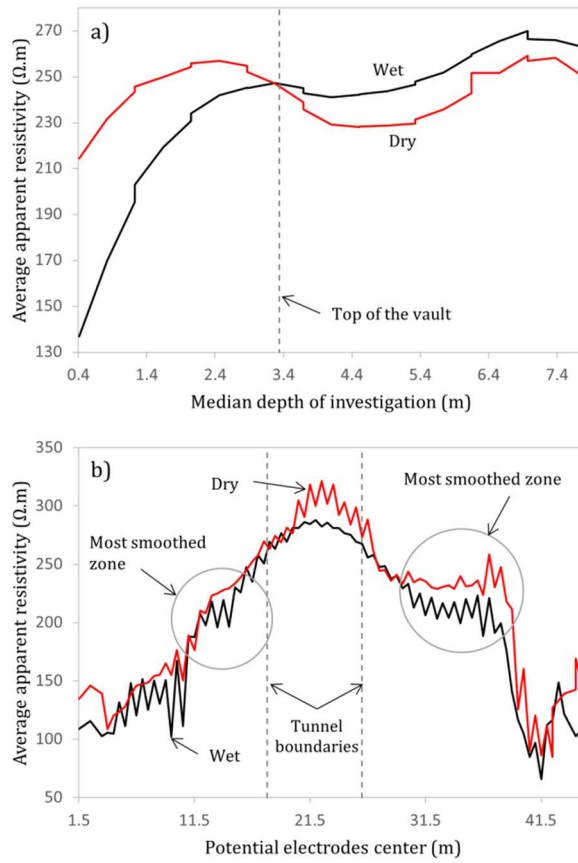
590

591

Fig. 9: Inverse resistivity model of the measured apparent resistivity under a) wet and b) dry conditions. The

592

tunnel's position is indicated on the profiles.



593

594

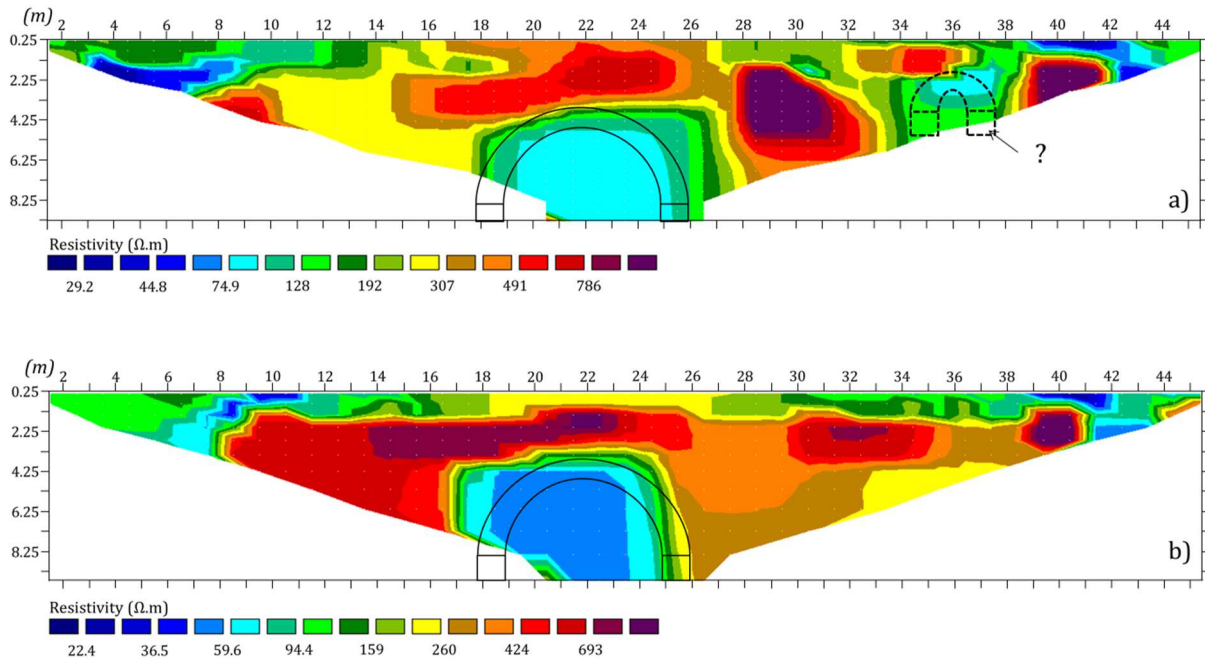
595 **Fig. 10:** Evolution of the averaged apparent resistivity after application of a smoothing filter in function of a)

596

the median depth of investigation and b) the potential electrodes center.

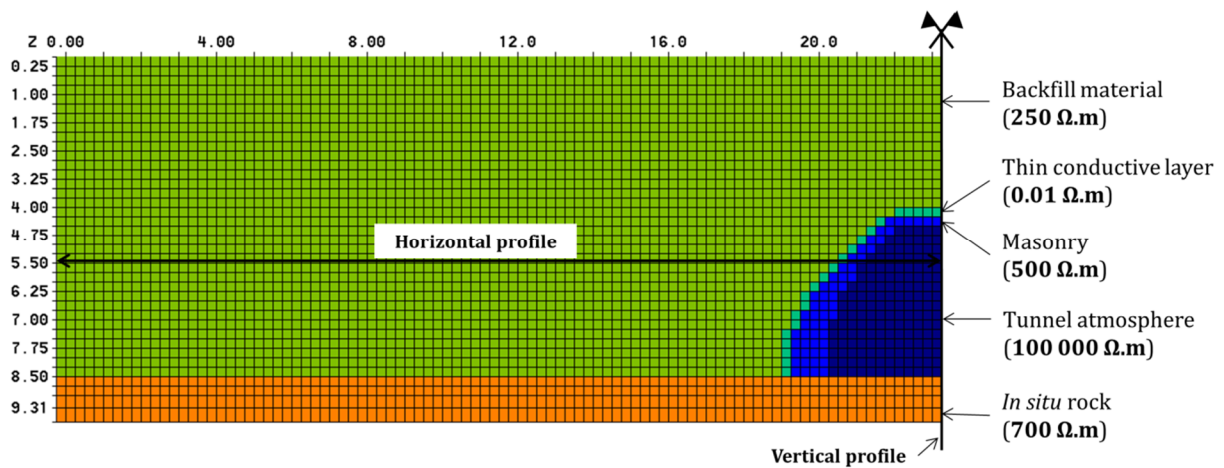
597

598



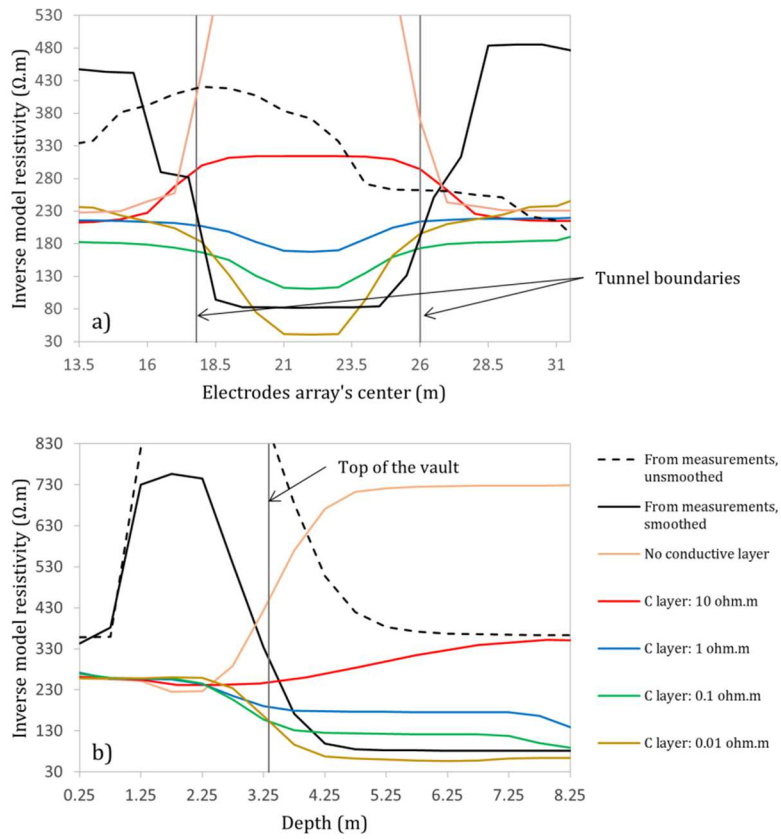
599

600 **Fig. 11:** Inverse resistivity model of the filtered (smoothed) apparent resistivity under a) wet and b) dry
 601 conditions. The main tunnel's position is indicated on the profiles and a position for the small secondary tunnel
 602 is supposed in case a).
 603



604

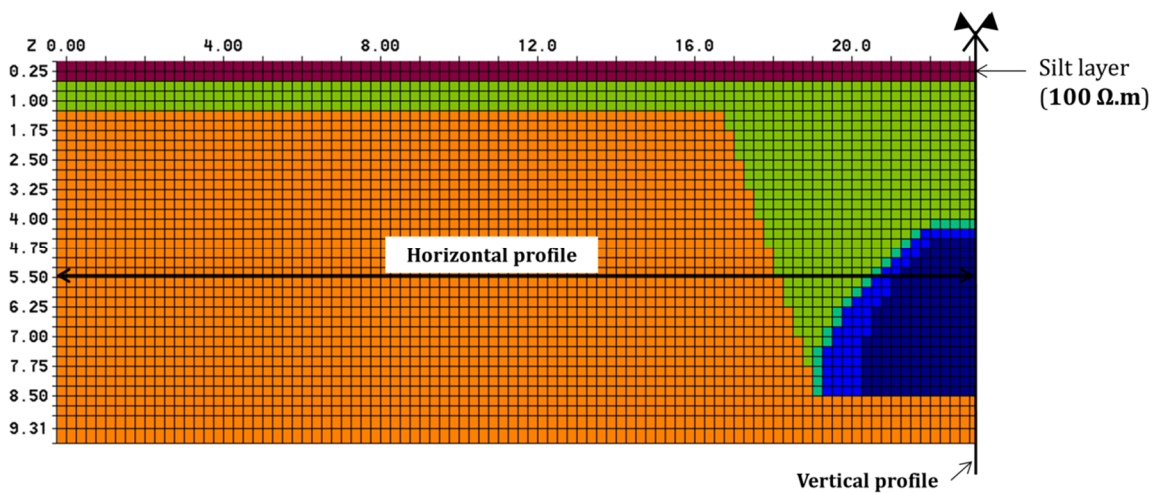
605 **Fig. 12:** Geometry of the first synthetic model (RES2DMOD).
 606



607

608 **Fig. 13:** Comparison of the inverse model resistivity obtained considering the field measurements (averaging
 609 the wet and dry resistivity, black curves) and considering the synthetic (RES2DMOD) models (color curves) with
 610 a variable resistivity of the thin conductive layer, a) along a horizontal profile at mid-height of the tunnel and b)
 611 along a vertical profile at mid-span of the tunnel.

612

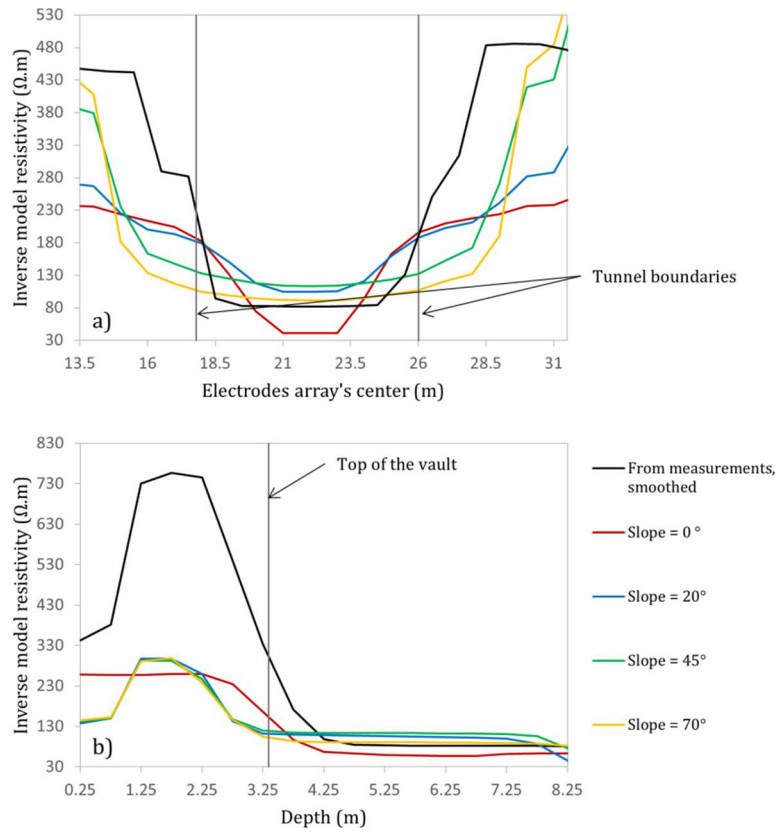


613

614

Fig. 14: Geometry of the second synthetic model (RES2DMOD).

615



616

617 **Fig. 15:** Comparison of the inverse model resistivity obtained considering the field measurements (averaging
 618 the wet and dry resistivity, black curve) and considering the synthetic (RES2DMOD) models (color curves) with
 619 a variable rock slope angle, a) along a horizontal profile at mid-height of the tunnel and b) along a vertical
 620 profile at mid-span of the tunnel.

621